Supplement of The Cryosphere, 20, 6809–6826, 2026
https://doi.org/10.5194/tc-20-6809-2026-supplement
© Author(s) 2026. CC BY 4.0 License.



The Cryosphere Open Access EGU

Supplement of

Impacts of snowpack on winter ecosystem respiration across the Northern Hemisphere

Bo Tang et al.

Correspondence to: Pengfeng Xiao (xiaopf@nju.edu.cn)

The copyright of individual parts of the supplement might differ from the article licence.

S1 Supplementary Methods

S1.1 Calculation of Snowpack Phenology

The duration spanning from 1 August of the present year to 31 July of the following year is termed a snowpack year, in accordance with the seasonal variations in snowpack in the NH [3, 6]. To reduce the effect of ephemeral snow on snowpack duration, the consecutive 5-day method is applied to extract SOD and SED by using daily snowpack depth data [2, 8]. The snowpack onset date was defined as the first day of the first five consecutive days of snowpack presence within each snowpack year (Equation S1), the snowpack end date was defined as the final day of the last five consecutive days of snowpack presence within each snowpack year (Equation S2), and the snowpack duration was defined as the number of days between the snowpack onset date and the snowpack end date.

$$Snowpack\ onset\ date = \min\{t\} \mid \left\{ t \in [0, m-4]\ and\ \sum_{k=0}^{4} S_{t+k} = 5 \right\} \tag{S1}$$

$$Snowpack\ end\ date = \max\{t\} + 4 \mid \left\{ t \in [0, m-4]\ and\ \sum_{k=0}^{4} S_{t+k} = 5 \right\} \tag{S2}$$

where t represents a date, m is the number of dates in a snowpack year, and S_t represents the value of a pixel, with 0 meaning non-snowpack and 1 meaning snowpack.

S1.2 Partial correlation analysis

Partial correlation analysis controls the effects of other correlated variables and measures the linear relationship between two variables, while the magnitude of the correlation is usually expressed as a partial correlation coefficient, which ranges from -1 to 1. The formula is as follows:

$$r_{xy,z} = \frac{r_{xy} - r_{xz} \cdot r_{yz}}{\sqrt{(1 - r_{xz}^2)(1 - r_{yz}^2)}} \tag{S3}$$

where r_{xy}, r_{xz}, and r_{yz} stand for the simple correlation coefficients (the zeroth-order partial correlation) between x, y, and z variables. $r_{xy,z}$ is the 1st-order partial correlation coefficient between variable x and variable y, in controlling the impact of variable z. The nth-order partial correlation can be easily computed from (n - 1)th-order partial correlations. The t-test is usually used to test the significance of the partial correlation coefficients as follows:

$$t = \frac{\sqrt{(n-k-2)} \cdot r}{\sqrt{(1-r^2)}} \tag{S4}$$

where r is the partial correlation coefficient, n is the size of samples, k is the number of variables upon which we are conditioning, $n-k-2$ is the numerator of the radical. We would reject the hypothesis and conclude that there is a significant partial correlation between these two variables if the absolute value of the test statistic exceeded the critical value from the t-table evaluated at $\alpha = 0.05$ over 2:

$$|t| > t_{n-2-c,\alpha/2} \tag{S5}$$

S1.3 Calculation of the Sign-Combination Statistics in Figures S16 and S17

Figure S16 summarizes, for each snowpack indicator (snowpack depth, snowpack duration, and snowpack density), the joint direction of the two sequential partial-correlation linkages examined in the snowpack insulation analysis: the linkage from the snowpack indicator to SII, and the linkage from SII to $\mathrm{Reco}_{\mathrm{winter}}$.

For every valid pixel (i.e., a pixel with a computable partial correlation coefficient for both linkages, shown as non-gray in Figure S15), the signs of the two partial correlation coefficients were cross-classified into four mutually exclusive and collectively exhaustive categories: (a) both linkages positive, (b) the first linkage positive and the second negative, (c) the first linkage negative and the second positive, and

(d) both linkages negative. Because these four categories partition all valid pixels, their area proportions sum to 100% for each snowpack indicator.

For each category, we report the area-weighted proportion of the total valid area at three significance levels, corresponding to the three bars shown from left to right in each panel of Figure S16: (i) all valid pixels, regardless of significance (All area); (ii) pixels in which at least one of the two linkages is statistically significant ($p < 0.05$); and (iii) pixels in which both linkages are statistically significant ($p < 0.05$). All proportions are area-weighted using the latitude weighting described below (Equation S7) and are expressed relative to the same denominator, namely the total valid area. Consequently, because tiers (ii) and (iii) are area subsets of tier (i), the proportion of a given category decreases monotonically as the significance criterion is tightened from tier (i) to tier (iii). Figure S17 complements these statistics by expressing, for the same four categories, the proportion of each significance subset occupied by each category, i.e., with each subset serving as its own denominator; the slices of each pie therefore sum to 100%.

S1.4 Calculation of Variable importance to prediction (VIP)

For a partial least squares regression model with m latent components where one seeks to predict y $(n \times 1)$ from X $(n \times p)$, the VIP value for the jth predictor is defined as follows:

$$VIP_j = \sqrt{\frac{p}{\sum_{h=1}^{m} R^2_{(y,t_h)}} \sum_{h=1}^{m} R^2_{(y,t_h)} w^2_{kj}} \tag{S6}$$

where $R^2_{(y,t_h)}$ is the proportion of the y variance explained by t_h.

S1.5 Latitude Weighting Methods

Due to the large latitudinal span of the study area (30°N - 90°N), the area of raster cells decreases significantly with increasing latitude. Directly counting the number of cells without projection transformation would overestimate the area proportion of high-latitude regions. We subsequently used a latitude-weighted averaging method to represent the area statistics, optimizing for differences in grid cell areas across different latitude ranges.

$$A_{i,j} = R^2 \cdot \cos(\varphi_i) \cdot \Delta\varphi \cdot \Delta\lambda. \tag{S7}$$

where $A_{i,j}$ is the actual area (km^2) of the pixel in the i-th row and j-th column; R is the average radius of the Earth (6371 km); φ_i is the latitude (rad) of the center of the pixel in the i-th row; $\Delta\varphi$ and $\Delta\lambda$ are the latitude and longitude resolution (rad) of the pixel, respectively.

S1.6 Soil Weighting Methods

The soil depth weighting formula and weighting are as follows:

$$T_{weighted} = \frac{\sum_{i=1}^{4} w_i \cdot T_i}{\sum_{i=1}^{4} w_i}. \tag{S8}$$

Where $T_{weighted}$ represents the average soil state, T_i represents the value corresponding to the current soil layer, and w_i represents the weight of the current soil layer.

S2 Supplementary Tables

S3 Supplementary Figures

Table S1. Information of Soil layering and weight allocation.

Soil layer	Depth range	Thickness	Weight
1	0–7 cm	7 cm	0.0242
2	7–28 cm	21 cm	0.0727
3	28–100 cm	72 cm	0.2491
4	100–289 cm	189 cm	0.6540

Table S2. Dataset details

Type	**Variable**	**Source**	**Citation**
Snowpack	Snowpack depth	ERA5-Land	[7]
	Snowpack density	ERA5-Land	[7]
	Snowmelt	ERA5-Land	[7]
Respiration	Ecosystem respiration	FLUXCOM	[5]
	Ecosystem respiration	BEPS	[4]
	Ecosystem respiration	LGS	[9]
Climate	Air temperature	ERA5-Land	[7]
	Precipitation	ERA5-Land	[7]
	Solar radiation	ERA5-Land	[7]
	Wind speed	ERA5-Land	[7]
Soil	Soil water content	ERA5-Land	[7]
	Soil temperature	ERA5-Land	[7]
Land cover		CCI-LC	[1]
Aridity index		Global Aridity Index and Potential Evapotranspiration Database - Version 3	[10]

Table S3. Description of snow station observation datasets.

Country	Data Source
Canada	CanSWE v6 (Environment and Climate Change Canada)
United States	USDA NRCS Snow Survey & SNOTEL Maine Geological Survey Northeast Regional Climate Center (NRCC) U.S. National Snow & Ice Center New Hampshire DES Dams
Finland	Finnish Environmental Institute (SYKE)
Russia	All-Russia Research Institute of Hydrometeorological Information (RIHMI-WDC) FSU Snow Survey (Hydromet Service of USSR)
Norway	Norwegian Water Resources and Energy Directorate (NVE)
Switzerland	WSL / SLF (Institute for Snow and Avalanche Research)
France	FMA Weather Station & Col de Porte Observatory (CENACLAM Project)
Austria	Weisssee AWS (Kaunertal Research Site)
China	China Meteorological Administration, National Climate Center

Table S4. Variance inflation factor of snowpack indicators.

Snowpack indicator	VIF
SD	4.2
SDEN	3.8
SM	1.3
SOD	5.6
SDD	2.1
SED	5.9

Table S5. The significantly partial correlated proportions of snowpack indicators and $Reco_{winter}$.

	0.1°	0.25°	0.5°
Snowpack depth	22.49%	23.32%	20.45%
Snowpack density	9.91%	9.29%	10.17%
Snowpack duration	9.50%	10.95%	9.76%

Table S6. Hydrothermal classification rules for partial least squares structural equation models.

Moisture condition \ Thermal condition	Annual mean air temperature $\leq$ 0°C	Annual mean air temperature > 0°C
Aridity Index (AI) < 0.2	Cold and arid	Warm and arid
0.2 $\leq$ AI < 0.5	Cold and semi-arid	Warm and semi-arid
0.5 $\leq$ AI < 0.65	Cold and semi-humid	Warm and semi-humid
AI $\geq$ 0.65	Cold and humid	Warm and humid

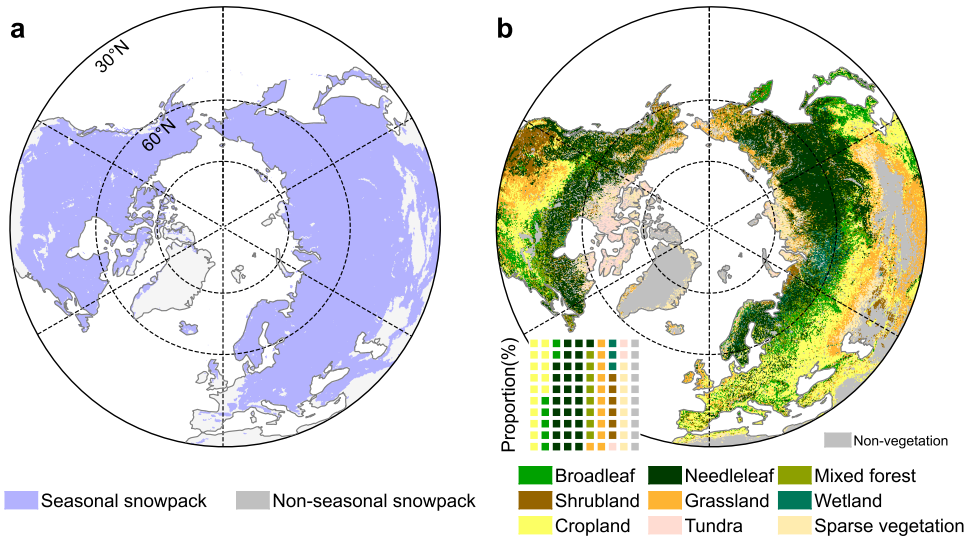

Figure S1. Spatial distribution of seasonal snowpack and vegetation types in the study area. The inset waffle in (b) indicates the proportion of the vegetation type in the Northern Hemisphere (> 30°N). Each pixel corresponds to 1%.

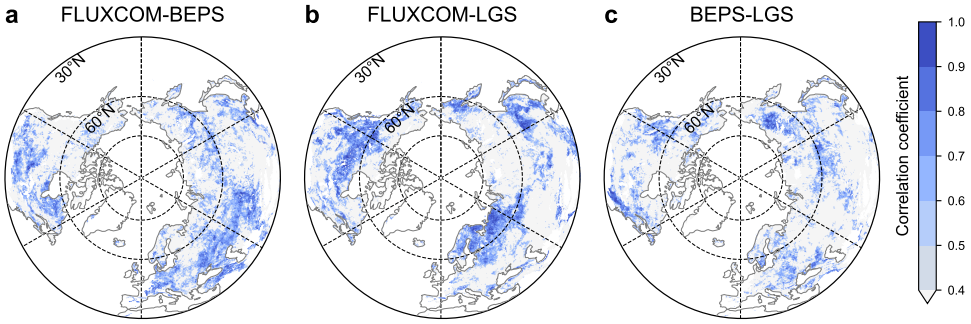

Figure S2. Comparison of the consistency between different ecosystem respiration datasets in the study area. a, b, and c indicate the correlation coefficient between FLUXCOM and BEPS, FLUXCOM and LGS, and BEPS and LGS, respectively. The correlation coefficients of all results are at a significance level of $p < 0.05$.

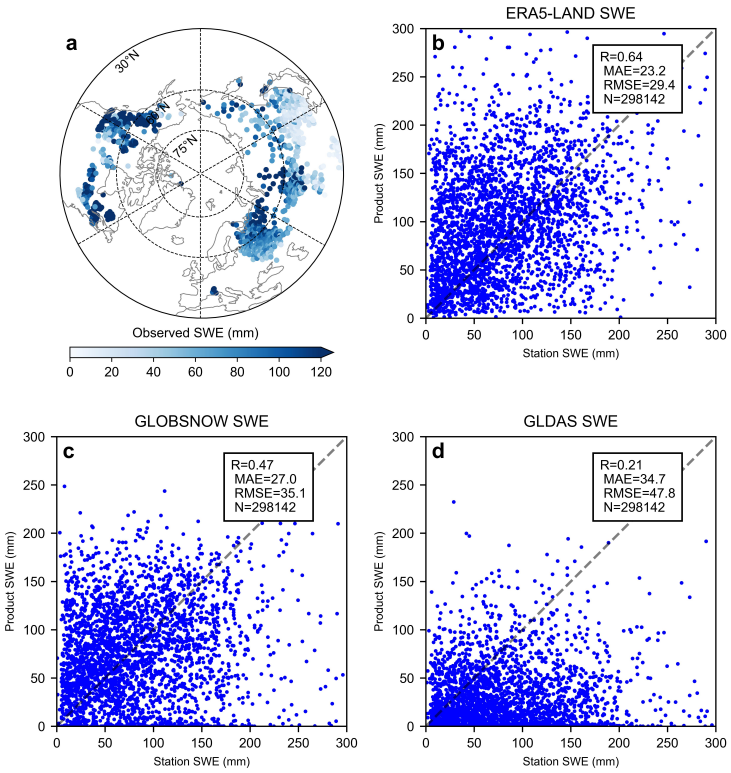

Figure S3. Comparison of ERA5-Land, GLOBSNOW, and GLDAS snow water equivalent products with station observations.

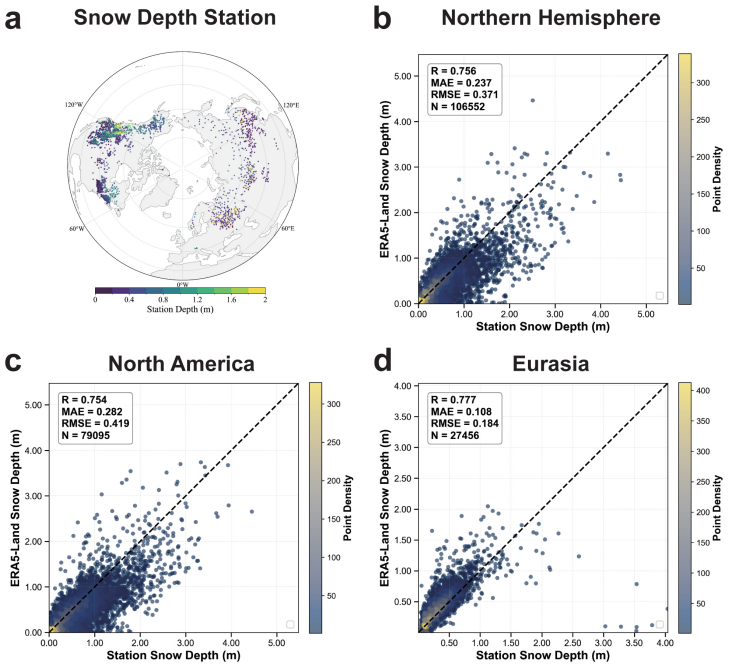

Figure S4. Comparison of ERA5-Land snow depth with station observations.

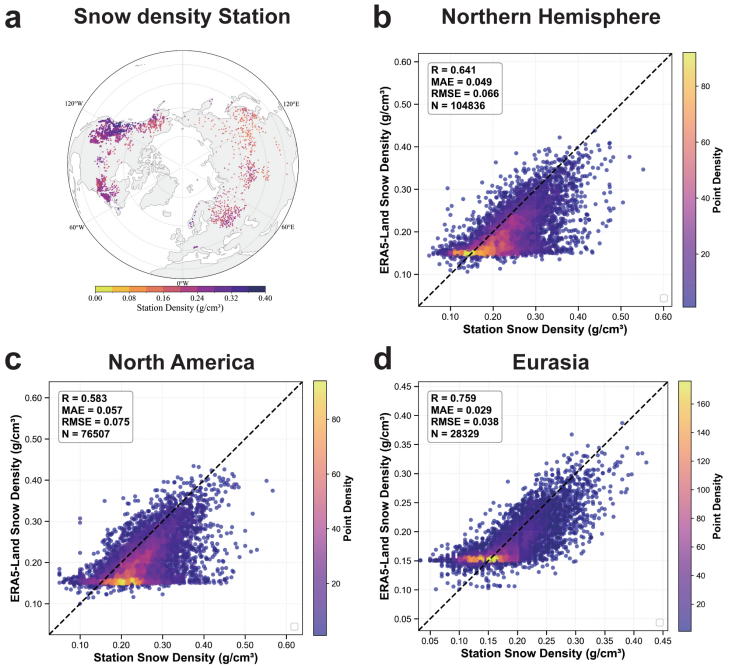

Figure S5. Comparison of ERA5-Land snow density with station observations.

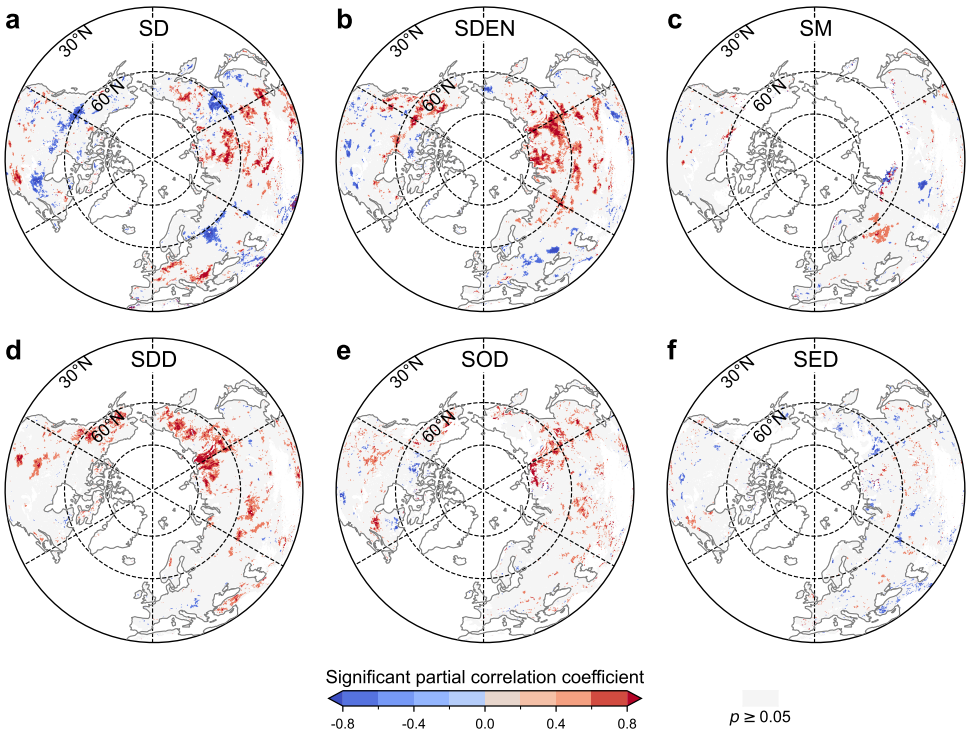

Figure S6. Spatial patterns of the significant partial correlation coefficients between the snowpack indicators and winter ecosystem respiration ($Reco_{winter}$) based on the BEPS dataset. The region shaded in gray denotes areas of non-significance ($p \geq 0.05$). SD, snowpack depth; SDEN, snowpack density; SM, total snowmelt; SDD, snowpack duration days; SOD, snowpack onset date; SED, snowpack end date.

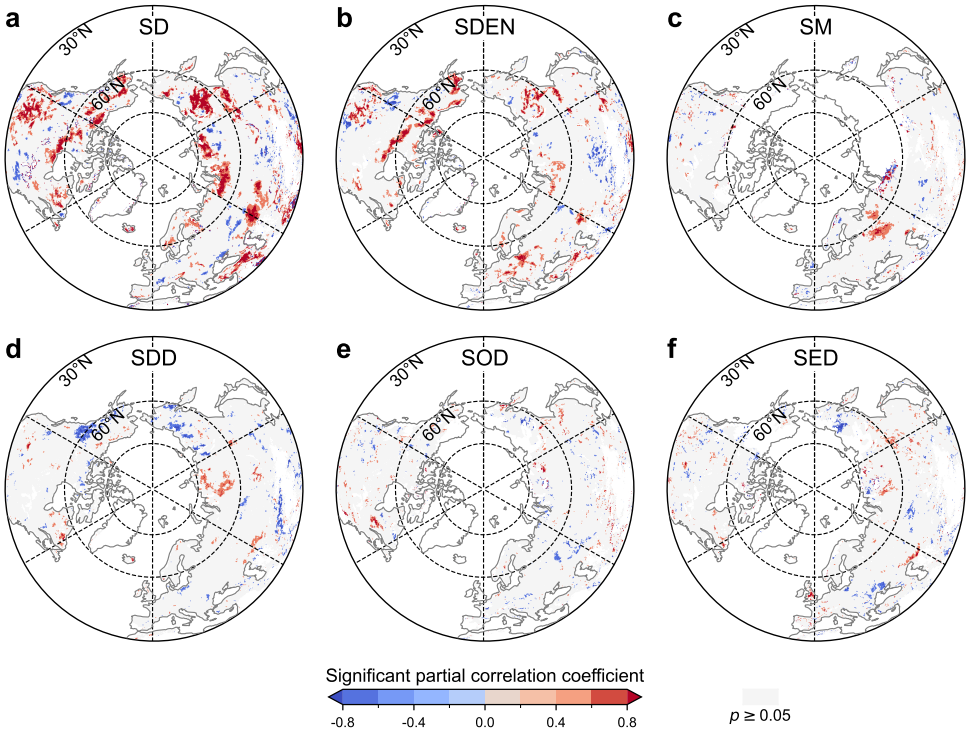

Figure S7. Spatial patterns of the significant partial correlation coefficients between the snowpack indicators and winter ecosystem respiration ($Reco_{winter}$) based on the LGS dataset. The region shaded in gray denotes areas of non-significance ($p \geq 0.05$). SD, snowpack depth; SDEN, snowpack density; SM, total snowmelt; SDD, snowpack duration days; SOD, snowpack onset date; SED, snowpack end date.

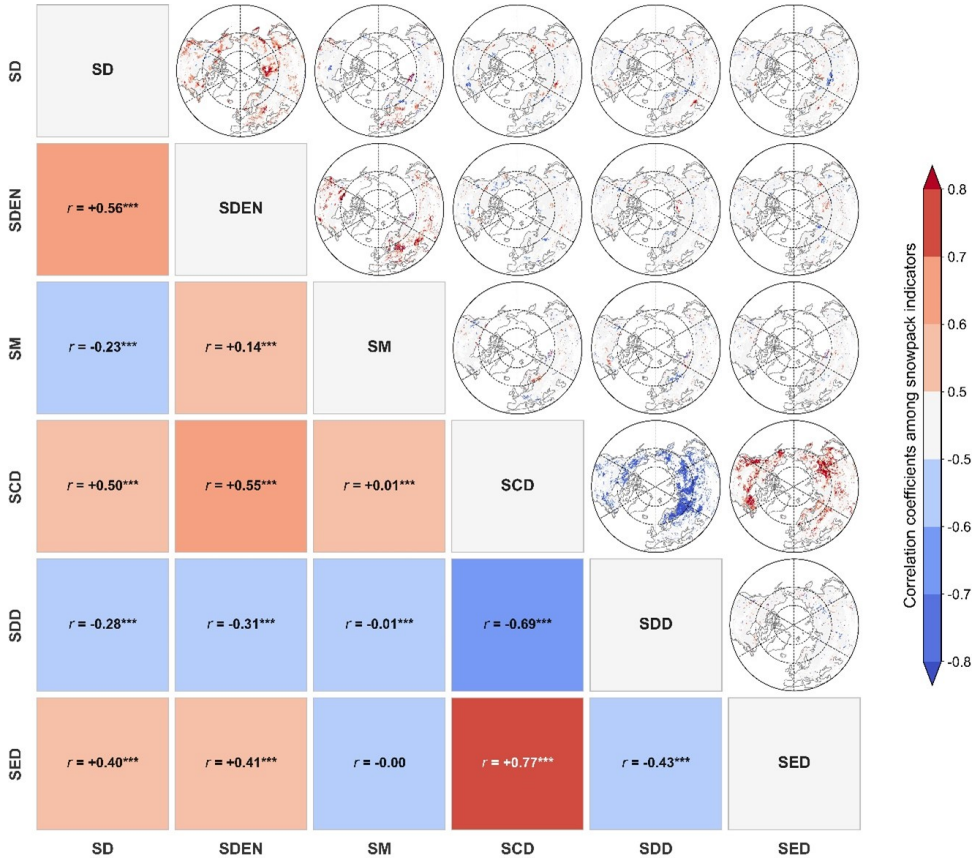

Figure S8. Correlation coefficients among snowpack indicators. The regions shaded in gray denote area of weak correlations. SD, snowpack depth; SDEN, snowpack density; SM, total snowmelt; SDD, snowpack duration days; SOD, snowpack onset date; SED, snowpack end date.

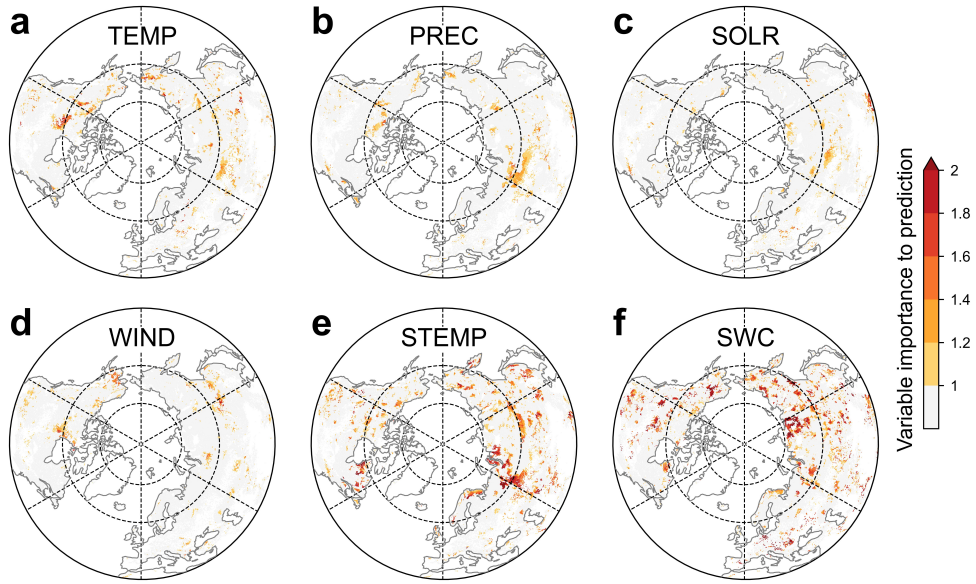

Figure S9. Spatial pattern of the VIP values of climate and soil indicators in partial least squares regression (PLSR) analysis. TEMP: air temperature, PREC: precipitation, SOLR: solar radiation, WIND: wind speed, STEMP: soil temperature, SWC: soil water content.

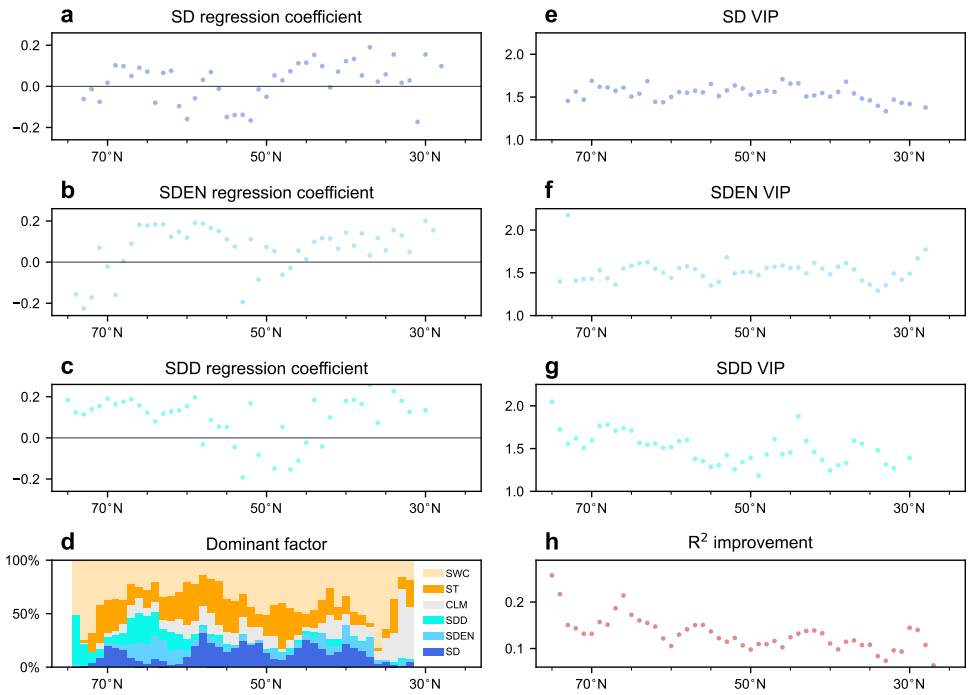

Figure S10. The impacts of snowpack on winter ecosystem respiration in relation to latitude. (a-c) Latitudinal distribution of regression coefficients of snowpack indicators in partial least squares regression (PLSR) analysis. Each dot represents the mean value of the regression coefficients between the snowpack indicators and $\mathrm{Reco_{winter}}$ in a specific interval of latitude. (d) Latitudinal distribution of the proportions of dominant indicators to $\mathrm{Reco_{winter}}$. Only intervals with more than 30 observations were retained. (e-g) Latitudinal distribution of variable importance to prediction (VIP) of snowpack indicators in PLSR analysis. (h) Improvements in determination coefficients (R^2) employing three snowpack indicators in the PLSR analysis across different latitudes. The latitude gradient is binned every 1 degree. SD, snowpack depth; SDEN, snowpack density; SDD, snowpack duration days; CLM, climate indicators; ST, soil temperature; SWC, soil water content.

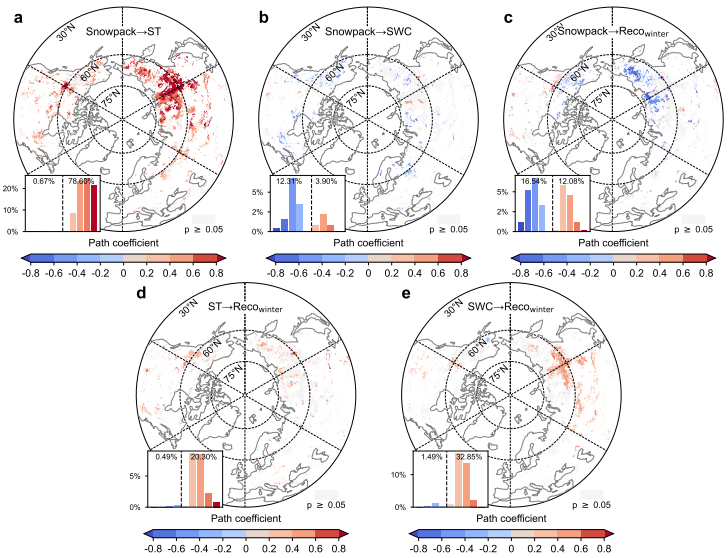

Figure S11. Spatial distribution of each segment of snowpack impacts on winter ecosystem respiration ($\mathrm{Reco_{winter}}$) derived from partial least squares structural equation models. The latent variable "Snowpack" is composed of snowpack depth, snowpack density, and snowpack duration days. The inset barplots indicate the proportions of negative and positive path coefficients in different intervals. The region shaded in gray denotes areas of non-significance ($p \geq 0.05$). ST, soil temperature; SWC, soil water content.

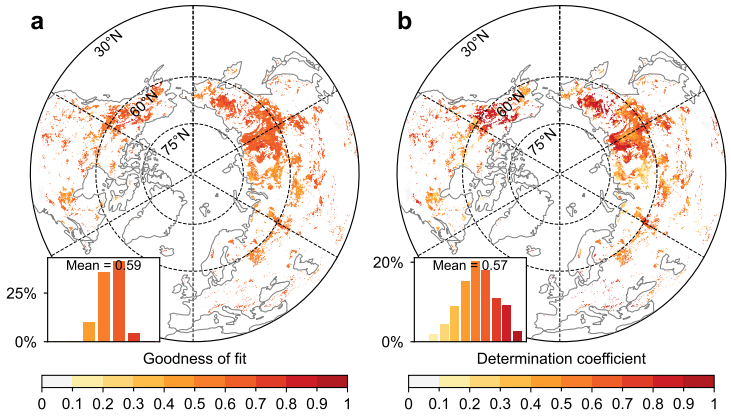

Figure S12. Spatial patterns of (a) the goodness-of-fit index, and (b) the determination coefficient of partial least squares structural equation model.

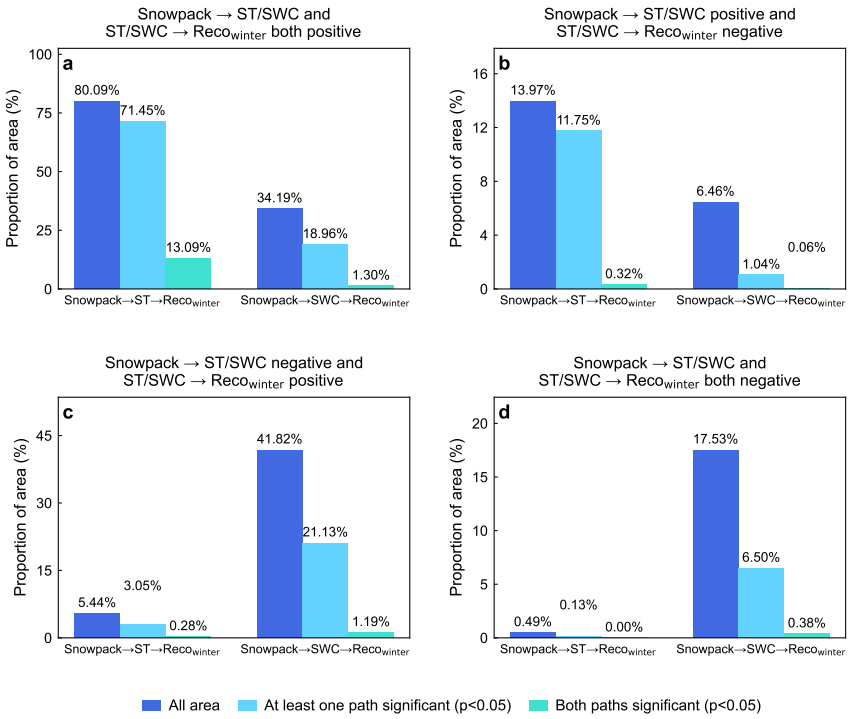

Figure S13. Area proportions of sign combinations between the two segments linking snowpack and winter ecosystem respiration ($\text{Reco}_{\text{winter}}$) through the thermal and moisture pathways. (a) Both segments are positive. (b) From Snowpack to ST/SWC is positive and from ST/SWC to $\text{Reco}_{\text{winter}}$ is negative. (c) From Snowpack to ST/SWC is negative and from ST/SWC to $\text{Reco}_{\text{winter}}$ is positive. (d) Both segments are negative. For each pathway, bars from left to right denote the area-weighted proportions of the total valid area with the given sign combination (All area), with at least one segment statistically significant ($p < 0.05$), and with both segments statistically significant ($p < 0.05$). ST, soil temperature; SWC, soil water content.

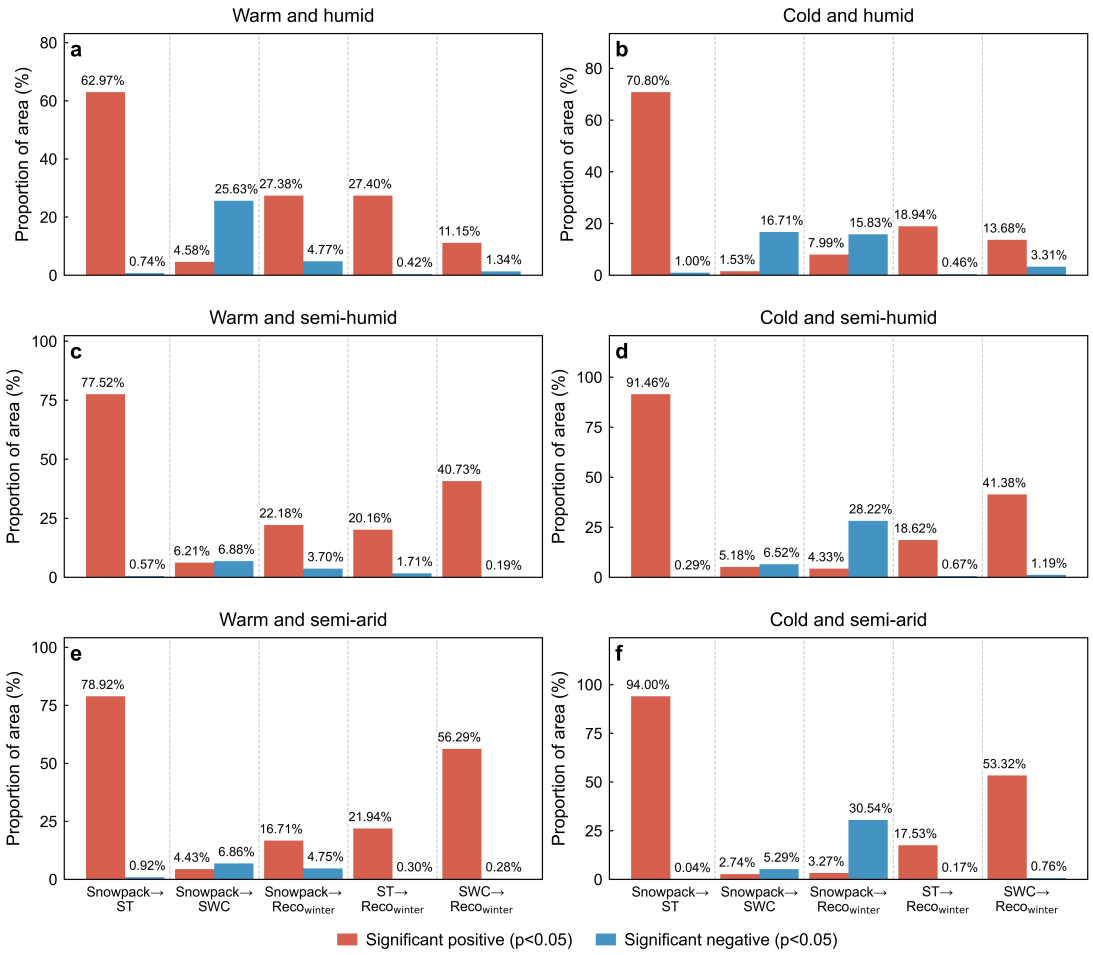

Figure S14. Area proportions of significant path coefficients for each segment of the snowpack impact pathways within each hydrothermal zone, derived from the pixel-level partial least squares structural equation models. (a) Warm and humid, (b) cold and humid, (c) warm and semi-humid, (d) cold and semi-humid, (e) warm and semi-arid, and (f) cold and semi-arid zones. For each segment, the red and blue bars denote the area-weighted proportions of pixels with significant positive and significant negative path coefficients ($p < 0.05$), respectively. The hydrothermal zones are classified by annual mean air temperature and aridity index (Table S6). ST, soil temperature; SWC, soil water content.

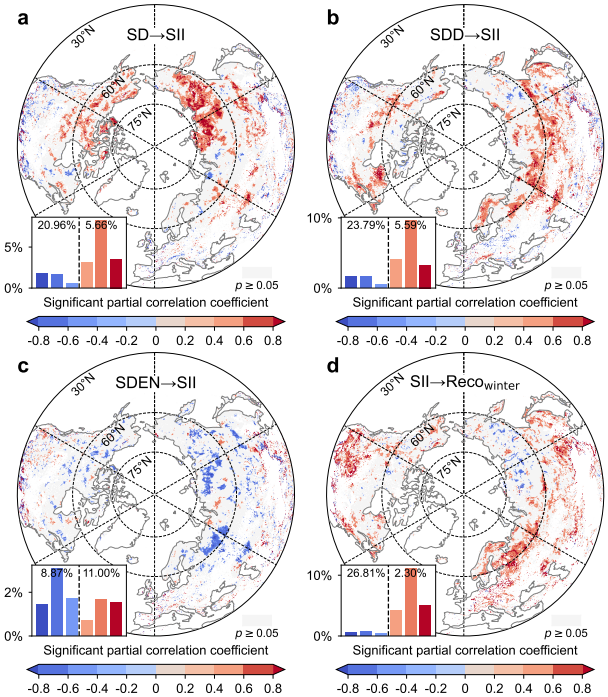

Figure S15. Spatial patterns of partial correlation coefficients between snowpack insulation and winter ecosystem respiration ($Reco_{winter}$). (a-c) The partial correlation coefficients between snowpack indicators and snowpack insulation indicator. (d) The partial correlation coefficients between snowpack insulation indicator and $Reco_{winter}$. The region shaded in gray denotes areas of non-significance ($p \geq 0.05$). SD, snowpack depth; SDEN, snowpack density; SDD, snowpack duration days. SII, snowpack insulation indicator.

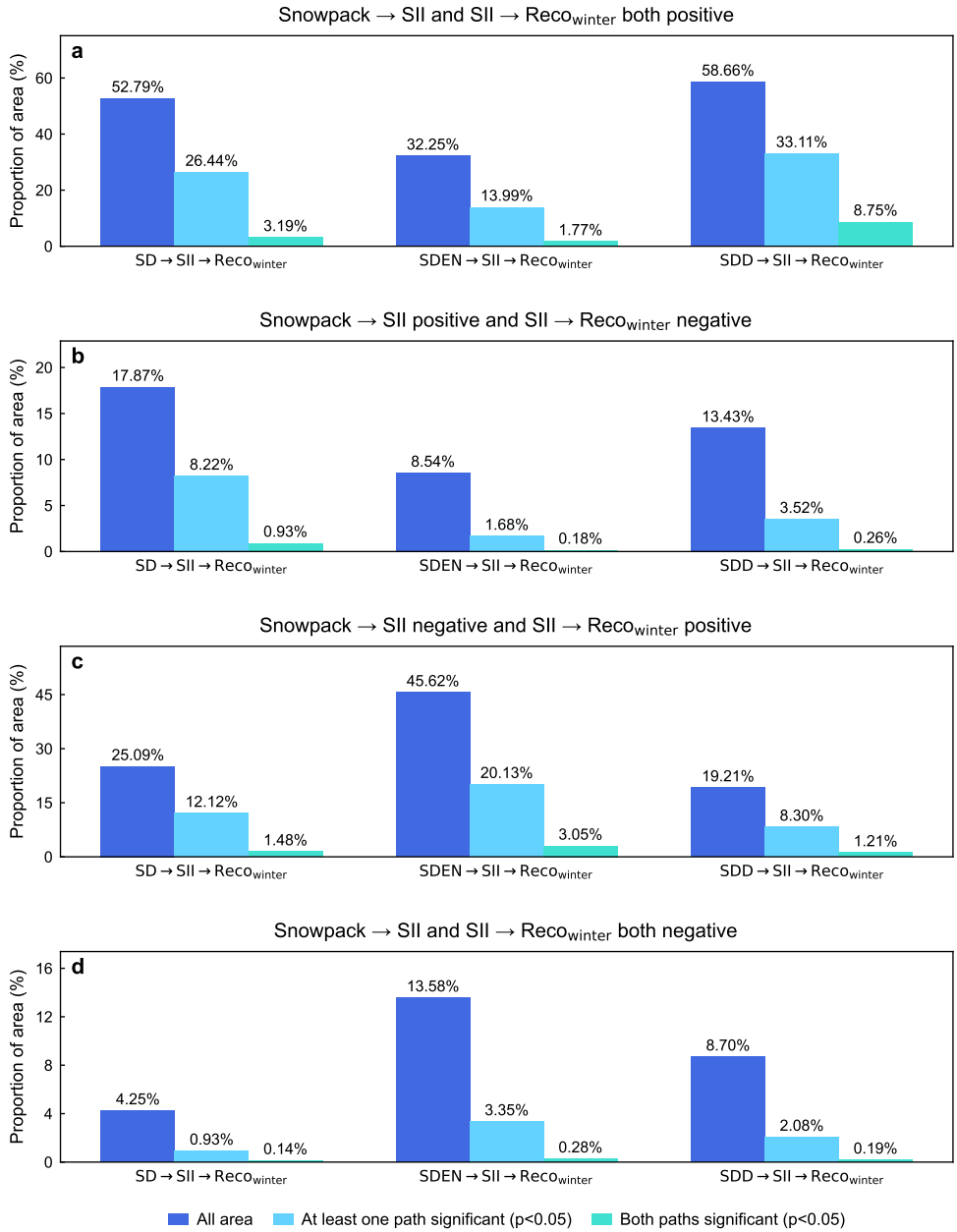

Figure S16. Area proportions of sign combinations between the two paths linking snowpack indicators and winter ecosystem respiration (Reco$_{winter}$). (a) Both paths (from Snowpack to SII and from SII to Reco$_{winter}$) are positive. (b) From Snowpack to SII is positive and from SII to Reco$_{winter}$ is negative. (c) From Snowpack to SII is negative and from SII to Reco$_{winter}$ is positive. (d) Both paths are negative. For each snowpack indicator, bars from left to right denote the area-weighted proportions of the total valid area with the given sign combination (all area), with at least one path statistically significant (p ¡ 0.05), and with both paths statistically significant (p ¡ 0.05). SD, snowpack depth; SDEN, snowpack density; SDD, snowpack duration days; SII, snowpack insulation indicator.

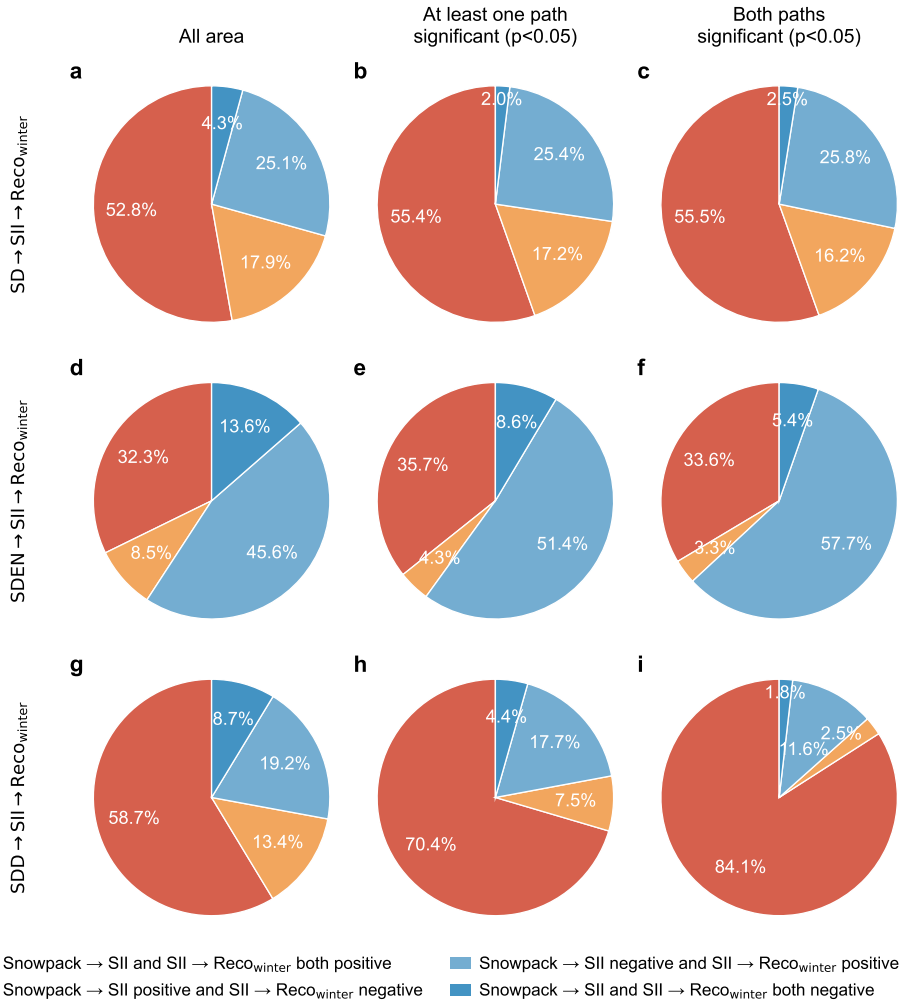

Figure S17. Proportions of the four sign-combination categories within each significance subset for the two sequential linkages between snowpack indicators and winter ecosystem respiration ($\mathrm{Reco_{winter}}$). Within each pie, the slices denote the proportion of the corresponding subset occupied by each category. SD, snowpack depth; SDEN, snowpack density; SDD, snowpack duration days; SII, snowpack insulation indicator.

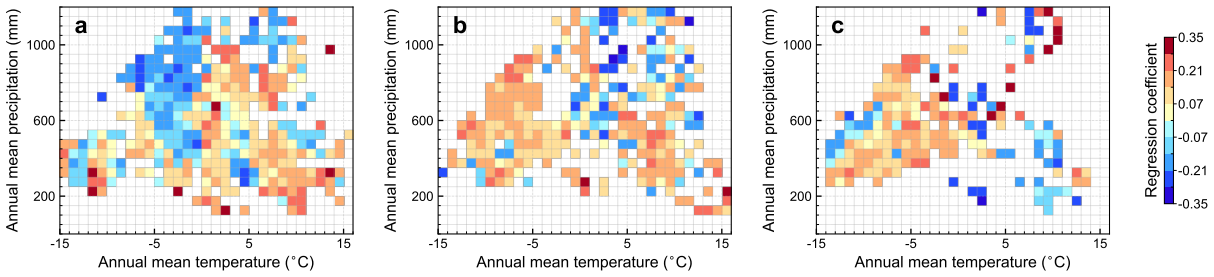

Figure S18. Variations in the regression coefficients between snowpack indicators and winter ecosystem respiration ($\mathrm{Reco_{winter}}$) along temperature and precipitation gradients. Each zone represents the mean value of the regression coefficients of the snowpack indicators in PLSR analysis in a specific interval of annual mean air temperature and precipitation. Only zones over 30 observations were retained. The mean annual air temperature and precipitation gradients are binned every 1°C and 50 mm, respectively. SD, snowpack depth; SDEN, snowpack density; SDD, snowpack duration days.

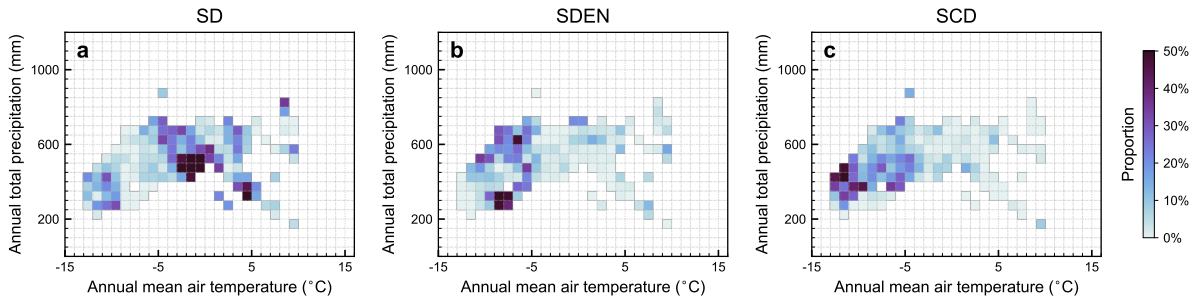

Figure S19. The proportions of snowpack indicators as dominant indicators for winter ecosystem respiration ($Reco_{winter}$) along temperature and precipitation gradients. Only zones over 30 observations were retained. The mean annual air temperature and precipitation gradients are binned every 1°C and 50 mm, respectively. SD, snowpack depth; SDEN, snowpack density; SDD, snowpack duration days.

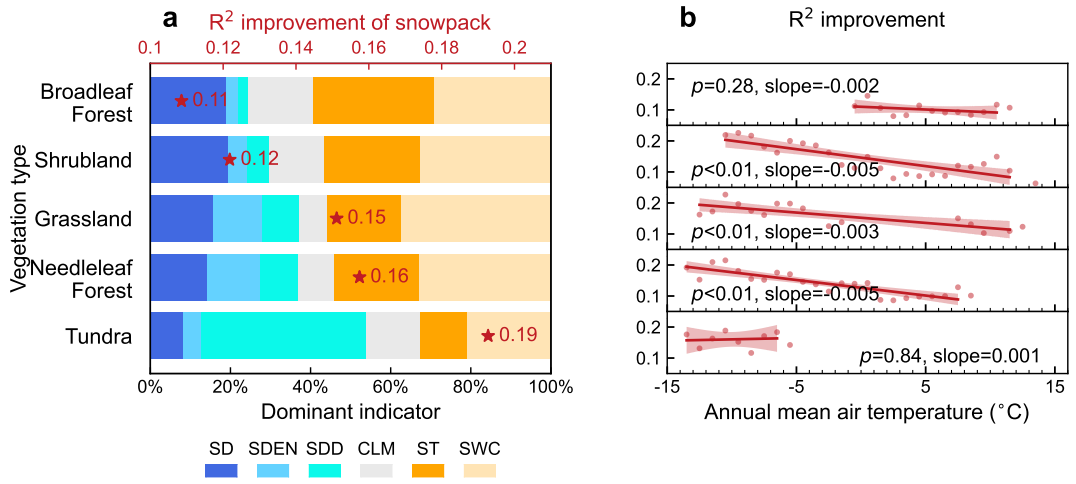

Figure S20. Variations in the significance of snowpack to winter ecosystem respiration ($Reco_{winter}$) among five main vegetation types. In (a), the stars with digits indicate the mean value of improvements in the determination coefficients (R^2) when multiple snowpack indicators are considered, and the bars represent the proportions of the dominant indicators for $Reco_{winter}$. In (b), the points represent the mean value of R^2 improvements along the temperature gradient among five vegetation types. The temperature gradients are binned every 1°C. SD, snowpack depth; SDEN, snowpack density; SDD, snowpack duration days; CLM, climate indicators; ST, soil temperature; SWC, soil water content.

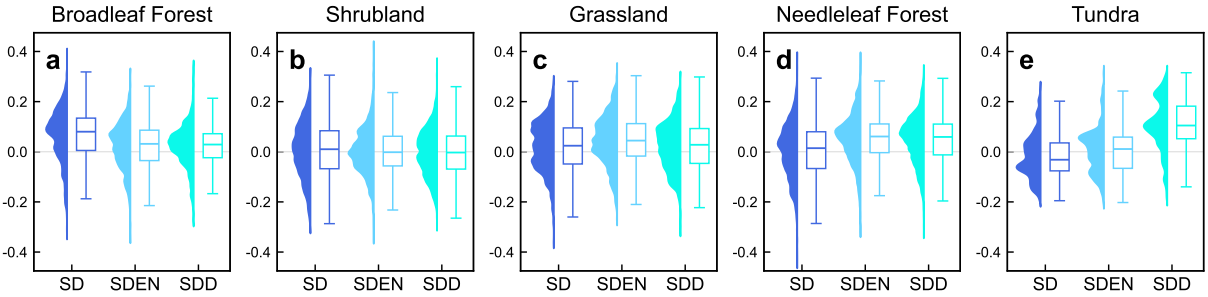

Figure S21. Variations in the relation between snowpack and winter ecosystem respiration ($Reco_{winter}$) among five main vegetation types (a. broadleaf forest, b. shrubland, c. grassland, d. needleleaf forest, and e. tundra). The left violin plots show the distributions of the regression coefficients of snowpack indicators in the per-pixel partial least squares regression analysis. The centerlines in the box plots indicate the median values, and the whiskers indicate the 1st/99th percentiles. The upper bars present the proportions of the dominant indicators in different vegetation types. SD, snowpack depth; SDEN, snowpack density; SDD, snowpack duration days.

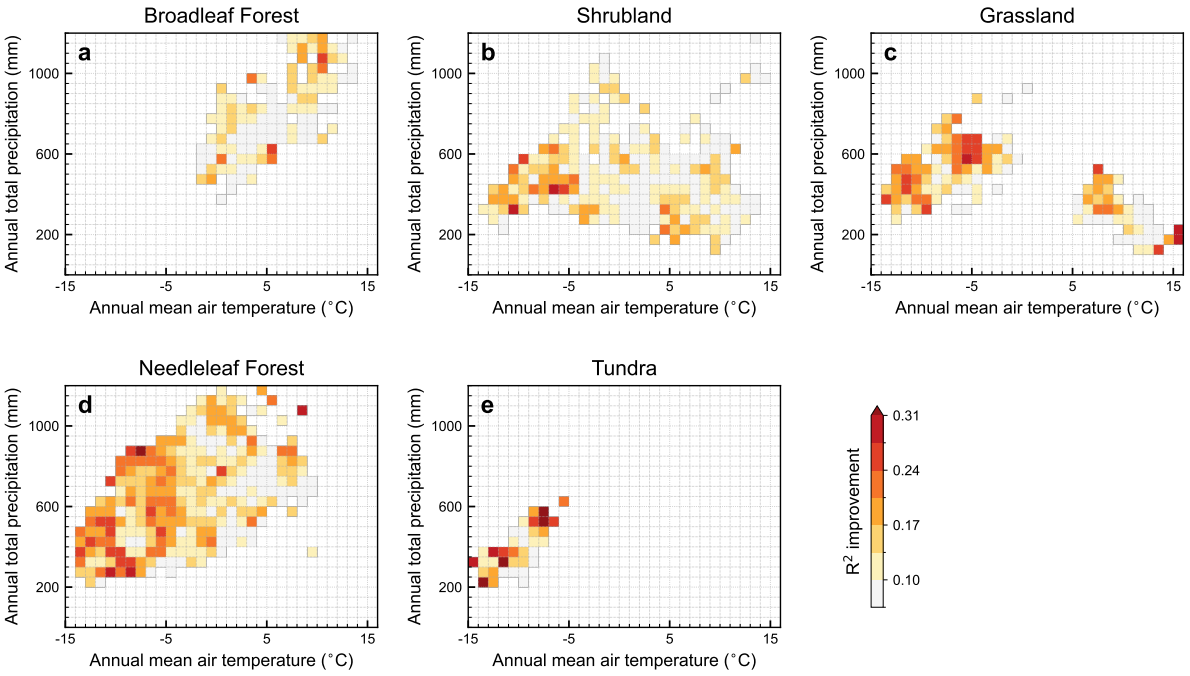

Figure S22. Variations in the significance of snowpack to winter ecosystem respiration ($Reco_{winter}$) along temperature and precipitation gradients among five main vegetation types (a. broadleaf forest, b. shrubland, c. grassland, d. needleleaf forest, and e. tundra). Each zone represents the mean value of improvements in the model determination coefficients (R^2) when multiple snowpack indicators are considered in a specific interval of temperature and precipitation gradients. Only intervals with more than 30 observations were retained. The temperature and precipitation gradients are binned every 1°C and 50 mm, respectively.

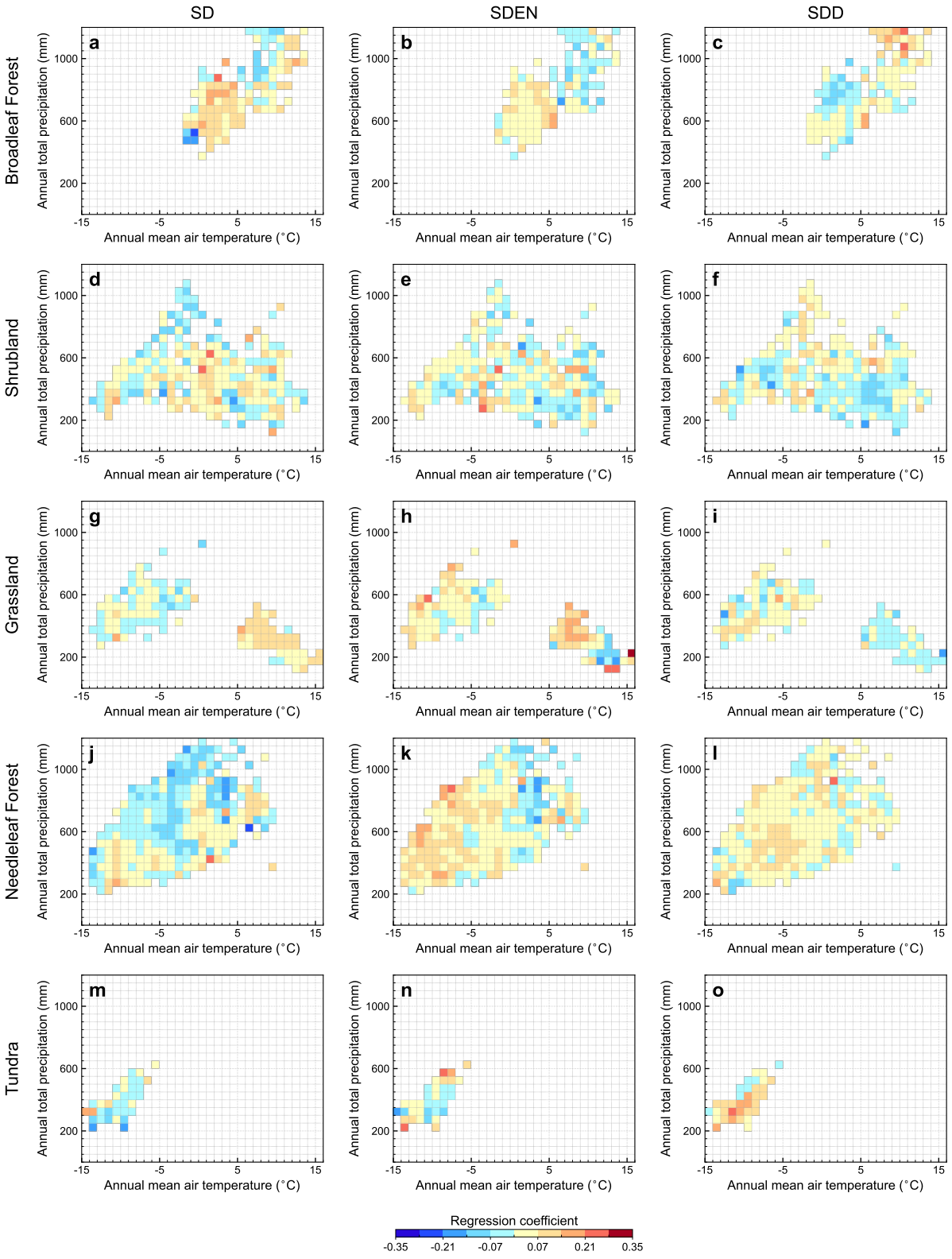

Figure S23. Variations in the regression coefficients between snowpack indicators and winter ecosystem respiration ($Reco_{winter}$) along temperature and precipitation gradients among five main vegetation types. Each zone represents the mean value of the regression coefficients between the snowpack indicators and $Reco_{winter}$ in a specific interval of annual mean air temperature and precipitation. Only intervals with more than 30 observations were retained. The mean annual air temperature and precipitation gradients are binned every 1°C and 50 mm, respectively. SD, snowpack depth; SDEN, snowpack density; SDD, snowpack duration days.

References

[1] ESA Land Cover CCI. Land cover cci product user guide version 2. *UCL-Geomatics: London, UK*, 2017. Available at: maps.elie.ucl.ac.be/CCI/viewer/download/ESACCI-LC-Ph2-PUGv2_2.0.pdf.

[2] Xiaona Chen, Shunlin Liang, Yunfeng Cao, Tao He, and Dongdong Wang. Observed contrast changes in snow cover phenology in northern middle and high latitudes from 2001–2014. *Scientific Reports*, 5(1):16820, 2015.

[3] Chunyu Dong. Remote sensing, hydrological modeling and in situ observations in snow cover research: A review. *Journal of Hydrology*, 561:573–583, 2018.

[4] Qiaoning He, Weimin Ju, Shengpei Dai, Wei He, Lian Song, Songhan Wang, Xinchuan Li, and Guangxiong Mao. Drought risk of global terrestrial gross primary productivity over the last 40 years detected by a remote sensing-driven process model. *Journal of Geophysical Research: Biogeosciences*, 126(6):e2020JG005944, 2021.

[5] Martin Jung, Sujan Koirala, Ulrich Weber, Kazuhito Ichii, Fabian Gans, Gustau Camps-Valls, Dario Papale, Christopher Schwalm, Gianluca Tramontana, and Markus Reichstein. The fluxcom ensemble of global land-atmosphere energy fluxes. *Scientific Data*, 6(1):74, 2019.

[6] Lawrence Mudryk, María Santolaria-Otín, Gerhard Krinner, Martin Ménégoz, Chris Derksen, Claire Brutel-Vuilmet, Mike Brady, and Richard Essery. Historical northern hemisphere snow cover trends and projected changes in the cmip6 multi-model ensemble. *The Cryosphere*, 14(7):2495–2514, 2020.

[7] Joaquín Muñoz-Sabater, Emanuel Dutra, Anna Agustí-Panareda, Clément Albergel, Gabriele Arduini, Gianpaolo Balsamo, Souhail Boussetta, Margarita Choulga, Shaun Harrigan, Hans Hersbach, et al. Era5-land: A state-of-the-art global reanalysis dataset for land applications. *Earth System Science Data*, 13(9):4349–4383, 2021.

[8] Shushi Peng, Shilong Piao, Philippe Ciais, Jingyun Fang, and Xuhui Wang. Change in winter snow depth and its impacts on vegetation in china. *Global Change Biology*, 16(11):3004–3013, 2010.

[9] Torbern Tagesson, Julia Kelly, Guy Schurgers, Feng Tian, Jonas Ardö, Stephanie Horion, Anders Ahlström, Stefan Olin, and Rasmus Fensholt. Increasing global ecosystem respiration between 1982 and 2015 from earth observation-based modelling. *Global Ecology and Biogeography*, 33(1):116–130, 2024.

[10] Robert J Zomer, Jianchu Xu, and Antonio Trabucco. Version 3 of the global aridity index and potential evapotranspiration database. *Scientific Data*, 9(1):409, 2022.